Variable Reluctance Rotating Shaft Sensor for DC Brushless Vernier Reluctance Motor

Bernard Multon, Marc Geoffroy, Pierre-François Desesquelles

VARIABLE RELUCTANCE ROTATING SHAFT SENSOR FOR D.C. BRUSHLESS VERNIER RELUCTANCE MOTOR

B.MULTON, M.GEOFFROY, P.F. DESESQUELLES
Laboratoire d'Electricité Signaux et Robotique (L.E.Si.R.) URA CNRS D1375
Ecole Normale Supérieure de Cachan
61 , avenue du président WILSON
F 94 235 CACHAN Cédex

1-INTRODUCTION

Today switched reluctance motors have a growing number of applications, which go from mass-production low-cost drives [2,3] (domestic appliances, car industry ...) to high efficiency drives [4,5,6] (aeronautics). The main reasons for this growth are that those electromagnetic structures are easy to build, which gives them great robustness, and also that since the supply is done through unidirectional current, the running safety is increased [6]. As those motors are brushless and self-commutated, the position of the rotor has to be known. It can be given by a direct sensor or an indirect sensor [7,8]. Direct sensors of optoelectronic technology or of Hall effect can be used for low-cost applications sensors of the resolver type are used for high efficiency applications but their cost is excessive compared to the motor's price, especially for low powers (<1kW). Regarding indirect sensors, they allow cost reduction and the suppression of shaft mechanical coupling, but there are still drawbacks in return, for instance at the start, at high speed, or again according to the king of control used (P.W.M or full wave modulation). In this paper, we suggest a third solution which consists in integrating the sensor into the motor. The structure of the motor is used to make a specific position sensor : a short pile of laminations similar to those of the motor's is put at the end of the active electromagnetic structure. The motor's and the sensor's stators are then assembled and put in a crank case, and both rotors are put on the same shaft. That constitutes an "integrated" sensor, which prevents the problem of mechanical coupling and its numerous consequences. Note that this solution is worthwhile for small motors only, because it seems inconceivable to build huge sensors for larger motors. Variable reluctance integrated sensors have already been built but their designers tried to reproduce the functioning of two-phase sine resolvers [9]. The main constraint is then to optimize the toothing shape in order to get sinusoidal permeance waves that permitted the use of "Resolver to Digital Converter" integrated circuits. In that case, the toothing of the sensor's magnetic circuit has to be different from the motor's. In this article, we suggest to determine the characteristics of the motor's magnetic circuit that permit to get signals required for self commutation. We will in particular show the great influence iron permeability can have on these characteristics.

2-PRINCIPLE OF THE VERNIER RELUCTANCE POSITION SENSOR

Figure 1 shows the electromagnetic structure of a motor and of its Vernier reluctance sensor.The structure represented is of the 6-4 type (6 poles for the stator and 3 phases, 4 poles for the rotor). The figure defines the main size parameters of the structure [10]. With the directions of the excitation ampere-turns of each phase that are indicated in figure 1, the flux equations for each phase can be written as follows :

$$\begin{aligned} \varphi_1 &= P_1(\theta).ni_1 + M_{21}(\theta)ni_2 + M_{31}(\theta).ni_3 \\ \varphi_2 &= P_2(\theta).ni_1 + M_{12}(\theta)ni_1 + M_{32}(\theta).ni_3 \\ \varphi_3 &= P_2(\theta).ni_1 + M_{13}(\theta)ni_1 + M_{23}(\theta).ni_2 \end{aligned} \qquad (2.1)$$

ni_i are the excitation ampere-turns for each phase ($i = 1$ to 3). P_i are the self permeances and M_{ij} the mutual permeances.Both $P_i$and M_{ij} are functions of the electrical angle θ, which is linked to the mechanical angle θ_m by : $\theta = N_r \cdot \theta_m$

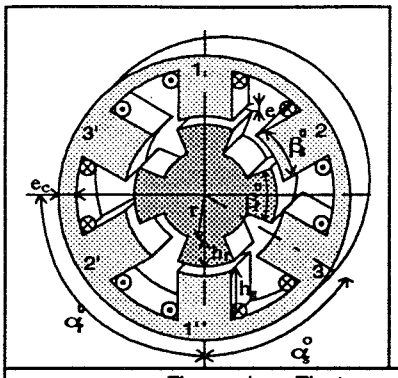

In our example, the working principle of the three-phase sensor consists in supplying all the phases connected in series with the same middle-frequency (around 10 kHz) alternating current. In these conditions, when the ampere-turns of the three phases equal n_i, the previous equation system (2.1) can be written as follows :

$$\begin{aligned} \varphi_1 &= (P_1(\theta) + M_{21}(\theta) + M_{31}(\theta)) .ni = P_{11}(\theta).ni \\ \varphi_2 &= (P_2(\theta) + M_{12}(\theta) + M_{32}(\theta)) .ni = P_{22}(\theta).ni \\ \varphi_3 &= (P_2(\theta) + M_{13}(\theta) + M_{23}(\theta)) .ni = P_{33}(\theta).ni \end{aligned} \qquad (2.2)$$

Figure -1- : Electromagnetic structure of the sensor (6-4 type)Main size parameters

Each self permeance is dephased of $2\pi/3$ in relation to the others and the mutual permeances respect a certain symmetry in order that : $M_{31}(\theta) = M_{21}(2\pi-\theta)$ (2.3)

Therefore, it is impossible that the three permeances P_{11}, P_{22} and P_{33} are made to be identical functions dephased of $2\pi/3$ in relation to one another. That phenomenon of dissymetry is a typical feature of certainVernier structures. However, the low values of the mutual permeances in comparison with the self permeances (see §3), as well as adequate current directions for the three phases, allow the reduction of dissymetry, which then goes unnoticed. This assumption will be justified by finite element field computation in Chapter 3 and by experiments in Chapter 4.

Figure 2 describes the principle of excitation and of electronic processing of the sensor's signals. Each phase winding is made up of two coils without dispersion. One of them is supplied with a sine excitation current while the other is used for detection and gives an induced voltage at the excitation frequency. The voltage amplitude is modulated by the position as well as by the speed. Indeed the induced voltage equation is composed of two terms whose amplitudes are respectively proportional to the permeance Pii(θ) (image of the position) and to the rotation speed (formula 2.7):

- let the excitation current be : $i = I_M \sin(\Omega_0 t)$ (2.4)

- the induced voltage at the terminals of the phase 1 is : $u_1 = n_2 . \dfrac{d(P_{11}(\theta) . n_1 i_1)}{d\theta} . \omega$ (2.5)

- the electric angular frequency equals : $\omega = N_R . \Omega$ (2.6)

in which N_R is the number of rotor teeth (4 in this case) and Ω is the rotation speed.

At steady state, equation (2.5) can be written as follows :

$$u_1 = n_2.n_1 I_M \sin(\Omega_0 t).\omega.\frac{d(P_{11}(\theta))}{d\theta} + n_2.n_1 P_{11}(\theta) .\Omega_0.I_M.\cos(\Omega_0.t) \qquad (2.7)$$

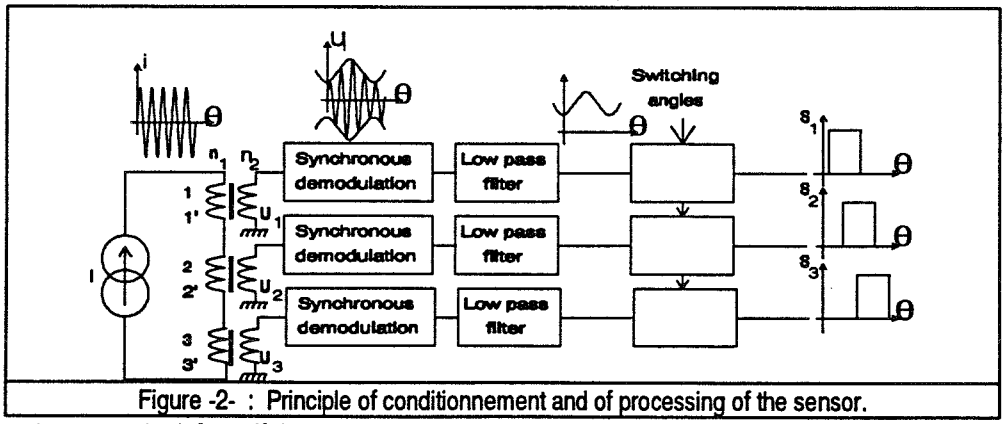

Figure -2- : Principle of conditionnement and of processing of the sensor.

The speed term can be left out if the speed remains under a certain limit that depends on the excitation frequency and the shape of the permeance wave according to (2.7).

In that case, a simple envelop detection can be enough to demodulate the induced voltage. In order to be free from the speed effect, a synchronous detection can turn out to be necessary. Beside, a second synchronous detection permits speed detection but that is not of interest in this article.

3 . ELECTROMAGNETIC STUDY OF THE SENSOR

We suggest to study the sensor by using a two-dimensional analytical calculation, which will be then compared with finite element numerical computation.Under the assumption that no saturation affects the sensor's magnetic circuit and that, self-permeances can be calculated. Mechanical angles are represented with the ° exponent so that electrical angles are given by $\theta = N_R \cdot \theta°$.

For each phase, the permeance linearly increases with the overlapping angle of the stator's and the rotor's teeth. Its minimum value P_0 is obtained at the unalined position and its maximum value P_c at the alined position. Since the field distribution obtained for the unalined position is rather complex, the value of P_0 has to be obtained by a finite element method. [11] showed that there are very few influential parameters : they are the $\frac{h_r}{S_r}$ and the $\frac{S_r}{W_s}$ ratios, in which W_s is the rotor booth's width, S_r the peak-to-peak rotor width at the air-gap level, and h_r the rotor tooth's height. As for the value of P_c , it can easily be calculated from the precise knowledge of the flux course if the air-gap is small. In this structure the flux path inside iron is long, moreover, at that low magnetic excitation level, the amplitude of iron permeability is rather small (μ_r=1000 or so for 4% silicon iron). For these reasons, the magnetic drop in the laminations has to be taken into account and the expression of P_c becomes :

$$P_c = \left(\frac{2.e}{\mu_0 . W_s . l} + R_{FE} \right)^{-1} \qquad (3.1)$$

R_{FE} is the total iron reluctance when the flux course in the stator's and rotor's teeth and in the yokes is taken into account :

$$R_{FE} = \frac{1}{\mu_0 . \mu_r . l} \cdot \left(\frac{\pi.(2.R_{ext} - e_c)}{4.e_c} + \frac{2.h_s}{W_s} + \frac{2.r}{W_r} \right) \qquad (3.2)$$

where R_{ext} is the exterior radius and w_r is the rotor pole width.

In order to validate this study, we have designed and built a prototype, whose size characteristics are as follows (see Figure 1) : r=16mm; h_s=11mm; h_r=5.9mm; e_c=4mm ; e=0.01mm; β_r=0.5; β_s=0.75

where $\beta_s = \frac{\beta_s^\circ}{\alpha_s^\circ}$ and $\beta_r = \frac{\beta_r^\circ}{\alpha_r^\circ}$ are the reduced pole angles.

With a magnetic circuit made of silicon iron (laminations 0.1mm ; μ_r = 1000), we obtained

P_0 = 36nH and P_c = 0.21μH

With a value of 1000 for μ_r (which corresponds to high excitation fields before saturation) the calculated value of P_c would have been 0.38 μH, and if the field circulation in iron had been left out, P_c would have equalled 0.48μH. The value of μ_r is consequently influential and cannot be omitted, although it is often done [9].

The idealized shape of the permeance wave is represented by a tapezoidal form. According to our analytical model, we suppose that, between the two extreme values of the permeance, the function P(θ) remains constant at the unalined position as long as a rotor tooth is not facing a stator tooth, that is during an electrical angle equal to :

$$\theta_{po} = 2\pi . \left((1-\beta_r) - \beta_s . \frac{N_r}{N_s} \right) \qquad (3.3)$$

Then the permeance linearly increases from P_0 to P_c during an electrical angle $D\theta_p$:

$$D\theta_p = 2\pi . \beta_s . \frac{N_r}{N_s} \qquad (3.4)$$

Finally, if the stator tooth angle β_s° is inferior to the rotor tooth angle β_r°, which is usually the case in switched reluctance motors [1], the permeance remains constant as long as the opposite surface is continuous, that is during an electrical angle θ_{po} equal to :

$$\theta_{pc} = 2\pi . \left(\beta_r - \beta_s . \frac{N_r}{N_s} \right) \qquad (3.5)$$

A two-dimensional finite element computation allows to accurately calculate the mutual permeances M_{ij} and to underscore the great importance of the relative permeability μ_r. Indeed for a rather high value of μ_r (4000),

interphase coupling effects are nearly insignificant. On the contrary, if μ_r equals 1000 (that is about for a low excitation level), coupling effects are considerable, and in particular they modify the shape of the total permeance P_{ii} (which includes the mutual permeances) and its peak-to-peak amplitude (see figures 3 and 5). The values of P_0 and P_c obtained thought finite element computation are respectively equal to 44nH (for any value of μr), and 0.38μH (μ_r=4000), 0.24μH (μ_r=1000), which is very close to what has been obtained with the previous method. Figure 3 shows a comparison between the two calculation methods of P_i in the particular case when the permeance wave has a triangular shape (θ_{po}=0, θ_{pc}=0, $D\theta_p$=π). This figure also shows the great influence the relative permeability can have on the shape of the self permeance wave and of the mutual permeance wave.

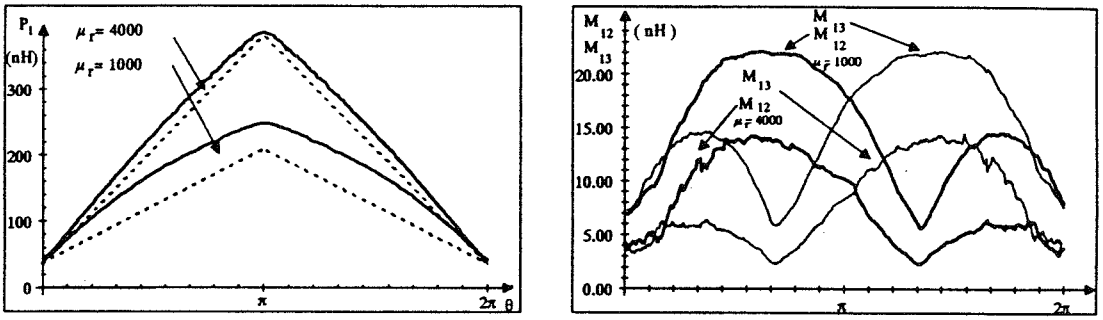

Figure -3- : Calculated wave shapes of the self permeance P_1
(dotted line for the analytical computation; continous line for the finite element method)
and (on the right) the mutual permeances M_{12} and M_{13} for μ_r=1000 and μ_r=4000

In practice, it was previously said that the three phases were connected in series and supplied with a unique current. Consequently the effective permeances are the P_{ii} defined by (2.2). The permeances have been calculated with the finite element method in the running conditions and figure 4 compares two field distributions, one obtained with single-phase supply, the other with a three-phase unique current.

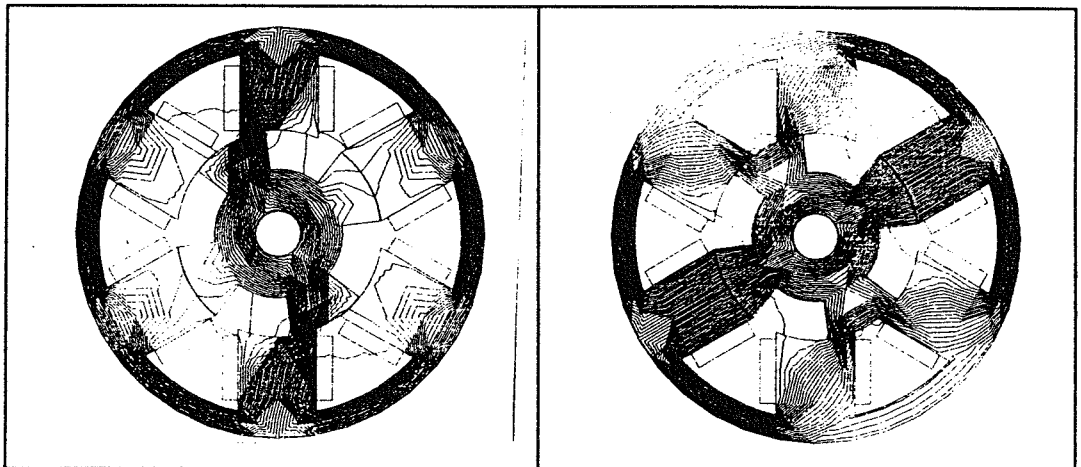

Figure -4- : Two dimensional field distributions for single-phase current (on the left) and three-phase series circuit (on the right)

We have compared the function $P_{11}(\theta)$ with the sum ($P_1(\theta)$ +$M_{21}(\theta)$ +$M_{31}(\theta)$) and noticed that the mutual permeances have an insignificant influence on the shape of the permeance wave only if the permeability is high enough (>4000). On the contrary, for smaller values of μ_r (1000 or less), the total permeance wave is very twisted and has a reduced amplitude . Figure 5 shows a comparison between the P_{ij} waveform calculated (with μ_r=500) and the P_{ij} measured. The latter have been calculated with the induced voltage values measured after synchronous demodulation (with 46 turns per phase (excitation and detection windings), an excitation current of 20 mA of

amplitude I_m at a frequency of 10 kHz). From the extreme values of the induced voltage amplitude , the values of the total permeances P_0 and P_c at unalined and alined positions have been calculated. They respectively equal 0,194 μH and 80 nH. Considering the unaccurate knowledge on the value of μ_r, the value of P_c has been rather well determined. On the contrary, the value of P_0, which has been calculated with the two-dimensional finite element method, has been underestimated with an error of -45% in comparison with the measurement.
A difference in amplitude at the alined position has been noticed for one of the three total permeances. It may be explained by the difference in lamination permeability according to the flux direction compared to the lamination direction.

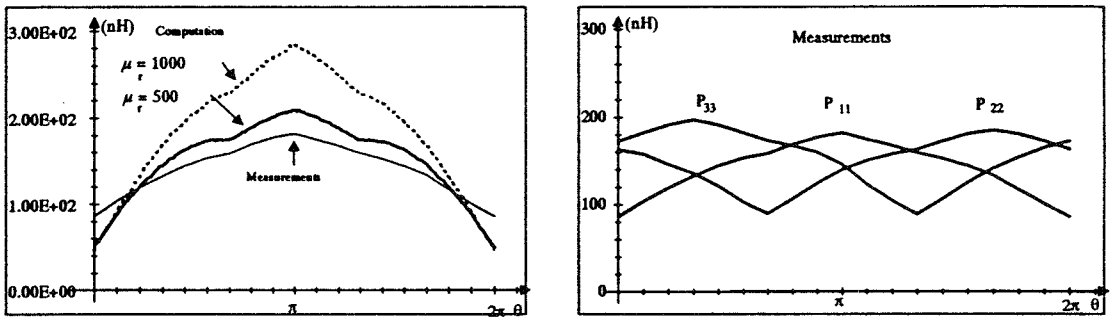

Figure 5 : Comparison between the functions $P_{ij}(\theta)$ measured and calculated (with μ_r=1000 and μ_r = 500).

4) THREE-DIMENSIONAL ANALYSIS

A three-dimensional finite element computation of the structure has been carried out and figure 7 shows the results of these calculations. The resulting inductance matrix gives the permeance of phase 1 (opposition) as : $P_o=\Sigma L_{1i}$=120nH.

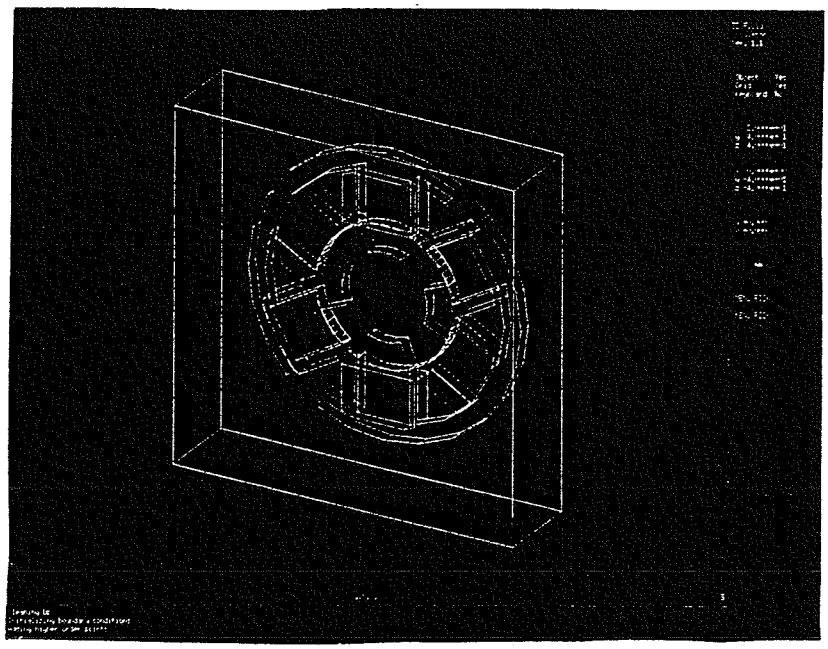

Figure 6 : 3-dimensional computation of the sensor's structure

inductance matrix

	b1	b1a	b2	b2a	b3	b3a
b1	9.09e-08	2.62e-09	-1.21e-08	2.58e-08	-1.21e-08	2.58e-08
b1a	2.62e-09	9.18e-08	2.61e-08	-1.22e-08	2.61e-08	-1.22e-08
b2	-1.21e-08	2.61e-08	2.27e-07	3.83e-08	-4.99e-08	7.99e-08
b2a	2.58e-08	-1.22e-08	3.83e-08	2.26e-07	7.99e-08	-4.99e-08
b3	-1.21e-08	2.61e-08	-4.99e-08	7.99e-08	2.27e-07	3.83e-08
b3a	2.58e-08	-1.22e-08	7.99e-08	-4.99e-08	3.83e-08	2.27e-07

3D calculation is not quite as reliable as 2D calculation. So we do not pay much attention to the exact value (120nH calculated versus 85 mesured); but this shows that end effects can not be neglected in the opposition position.

5) CONCLUSION

In this article, we have presented a low-cost position sensor aimed at the self-communation of small variable reluctance motors which uses the electromagnetic structure of the motor itself on a small width. A two-dimensional magnetic study has shown that the relative permeability of the magnetic amplitude had a considerable importance on the amplitude of the permeance wave (even for high values of μ_r), and on its shape if μ_r is small (lower 1000), which is the case when the excitation field is low. Moreover, interphase coupling effects cannot be left out as it has often been done before. The value of μ_r can absolutely not be supposed to be infinite and the main consequence is that the permeance wave is defined by the whole structure and not only by toothing shape.

Finally, the experiment of the prototype of a sensor has enabled us to verify our calculations. Differences between measurement and 2-dimensional calculations have been explained by end-effects that cannot be omitted for a short device and three-dimensional calculations have confirmed this assumption. Therefore, accurate predetermination of the characteristics of this very simple sensor requires precise electromagnetic computation and a good knowledge of the laminations permeability at low excitation level.

We thank the society L.P.M.I for the building and experiments of the sensor.

6) BIBLIOGRAPHY

[1] P.J. LAWRENSON, J.M. STEPHENSON, P.T. BLENKINSOP, J. CORDA N.N. FULTON "Variable- Speed Switched Reluctance Motors". Proceedings IEE, Vol. 127, Pt. B, No. 4, pp.253-265, July 1980.

[2] A. WELLER, P. TRAWINSKI, "Design and Control of Low Power Switched Reluctance Motors (< 1 KW)". EPE Firenze, 1991, pp. 4-001 to 4-006.

[3] B. MULTON, M. GABSI, "Influence de l'entrefer sur les performances et le dimensionnement d'un moteur à réluctance variable à double saillance et de son onduleur", 7éme colloque internat. sur les moteurs pas à pas, Nancy 1-3 juillet 1992.

[4] E. RICHTER, "Switched Reluctance Machines for High Performance Operations in Harsh Environment - A Review Paper". ICEM 1990, Vol. 1 pp. 18 à 24.

[5] D.A. TORREY, "A Comparison Between a Bifilar and a Monofilar High - Power Variable Reluctance Motor Drive", ICEM 1990, Vol. 1 pp. 60 à 65.

[6] A.V. RADUN, "High Power Density Switched Reluctance Motor Drive for Aerospace Applications", IEEE Trans.I.A. Vol.28, N°1, Jan./Feb. 1992, pp.113-119.

[7] N.H. MVUNGI, M.A. LAHOUD, J.M. STEPHENSON, "A new sensorless position detector for SR drives", Proc.IEE, 4 Int. Conf. on Power Elect. and Var. Sp. Dr., july 90, pp.249-252.

[8] S.K. PANDA, G.A.J. AMARATUNGA, "Switched Reluctance Motor Drive Without Direct Rotor Position Sensing", Annual meeting IAS-IEEE 1990, pp.525-530.

[9] D.C. HANSELMAN, R.E. THIBODEAU, D.J. SMITH, "Variable Reluctance Resolver Design Guidelines", proc. IE - CON'89, (Philadelphia) pp.203-208.

[10] B. MULTON, D. BONOT, J.M. HUBE, "Conception d'un moteur à réluctance autocommuté alimenté en courant", Congrès MOPP, EPFL Lausane 4/5 Juillet 1990,12p.

[11] D.P. TORMEY, D.A. TORREY, P.L. LEVIN, "Minimum Airgap-Permeance Data for the Doubly-Slotted Pole Structures Common in Variable-Reluctance-Motors". proc. IEEE IAS, Seattle Sept. 1990, pp. 196-200.